Deep learning based similarity-consistency abnormality detection (SCAD) model for classification of MRI patterns of multiple myeloma (MM) infiltration

Jinxin Zhou, Chuan Zhou, Heang-Ping Chan, Lubomir M. Hadjiiski, Qian Dong

(Department of Radiology, The University of Michigan, Ann Arbor, MI 48109-5842)

Purpose

Multiple myeloma (MM) is a common hematologic malignancy with high disease morbidity in the US. Studies indicated that the MRI patterns of MM infiltration are associated with tumor burden and correlated with prognosis in patients with MM. Because MM is a highly heterogeneous disease and large interpatient variability exists in MRI signals of the vertebras, it is a challenging task to identify the MRI patterns of MM, especially when the number of each subtype of MM patterns is small in the available training set. This study investigated the feasibility of classifying the MRI patterns of MM by developing a deep learning anomaly detection method trained with only the normal MRI pattern of MM.

METHOD AND MATERIALS

Using the generative adversarial network (GAN) as backbone that consisted of a generator (G) and a discriminator (D), we developed a similarity-consistency abnormality detection model (SCAD) for classification of MRI patterns that are associated with low and high risk of MM. Our SCAD model (Fig.1) consisted of two paths and three discriminators: generator-encoder (G-E) path, encoder-generator (E-G) path, discriminator D_{xz}, discriminator D_{xx}, and discriminator D_{zz}. Both paths used the same generator G and encoder E. In the adversarial training process, a batch of latent variables *z* randomly sampled from a Gaussian distribution was input to the G-E path, a batch of generated image patches G(z) and a batch of reconstructed latent variables E(G(z)) were sequentially output from the generator and encoder. Similarly, with a batch of image patches *x* from training set as input, the batches of encoded latent variables E(x) and

reconstructed images G(E(x)) were sequentially output from the E-G path. The discriminators D_{xz}, D_{xx}, and D_{zz} were optimized simultaneously to maximize three dissimilarity losses: (1) L_{xz}: loss of dissimilarity between (x, E(x)) and (G(z), z), (2) L_{xx}: loss of dissimilarity between (x, x) and (x, G(E(x)), and (3) L_{zz}: loss of dissimilarity between (z, z) and (z, E(G(z))). While the generator G and encoder E were also optimized together to minimize the three dissimilarity losses described above, we designed an additional loss L_{cycle} for the generator and the encoder to minimize the dissimilarity between the input patches and GAN-reconstructed patches, as well as their latent variables, which enabled the generator and encoder to be cycle-consistent ($\mathrm{G}(\mathrm{E}(x)) \approx x$ and $\mathrm{E}(\mathrm{G}(z)) \approx z$).

After the training of the SCAD, an inference architecture (Fig.2) was deployed to the test set. A test image x was input to the encoder E and obtained the corresponding latent variable. The latent variable was then fed to the generator G to generate a reconstructed image $\tilde{x}$. We designed a combined dissimilarity measures in image spatial domain and feature spaces as the abnormal score $\mathrm{A}(\mathrm{x})$ to quantify the differences between the input and the SCAD generated image.

$$\mathrm{A}(\mathrm{x}) = \|x - \tilde{x}\|_1 + \|f_{xx}(x, x) - f_{xx}(x, \tilde{x})\|_1$$

where f_{xx} were the features from the penultimate layer of discriminator D_{xx}.

With Institutional Review Board approval, a total of 132 sagittal views of T1-weighted (T1W) sequence in the spinal MRI scans was collected from 67 patients at our institution and used in this study. All scans were acquired with GE MR scanners. The pixel size of the T1W scans ranged from 0.532 mm to 1.797 mm in the sagittal plane. An experienced musculoskeletal radiologist manually outlined each vertebra and provided the descriptor of its patterns (normal, focal, variegated (salt-pepper) and diffused) as reference standard. For each marked vertebra, a region of interest (ROI) was manually cropped to enclose the region of the vertebra and its adjacent intervertebral discs as the training and test patch samples. A total of 1541 ROIs containing vertebras of normal MRI pattern associated with low risk of MM were extracted, and split into training and validation patches at a case ratio of 7:3. A total of 4553 ROIs of non-normal patterns associated with high risk of MM were extracted and used as an independent test set, in which 1679, 2044 and 830 vertebras, respectively, were identified as showing focal, variegated and diffuse patterns by radiologist.

Results:

The performance of the SCAD model in classification of MRI patterns was evaluated with the area under ROC curve (AUC) (Table 1). Our SCAD trained with normal vertebral patterns achieved a test AUC of 0.71, 0.79 and 0.87 in differentiating focal, variegated and diffuse patterns from the normal pattern, respectively, with an average test AUC of 0.77. In comparison with the Anogan and Ganomaly models reported in the literatures, the Anogan and Ganomaly achieved an average test AUC of 0.645 and 0.657, respectively, which are significantly lower than our SCAD model ($P<0.05$).

Conclusion:

The results demonstrated that our SCAD model could identify the MM patterns of vertebras in MRI with high accuracy, and provided higher classification accuracy than those of the Anogan and Ganomaly methods reported in the literature.

New or breakthrough work:

We developed a one-class semi-supervised deep learning model that can be trained with only normal cases and deployed to abnormal cases. Compared with conventional deep learning methods for multiclass classification that usually require a large number of multiclass cases for the training, a large number of normal cases is relatively easier to be collected from MM patients and even from MM-free patients to further train our one-class model in future studies. Instead of using a large number of abnormal cases to train a multiclass model, which could be difficult to collect from patients with a limited number of subtype diseases, the collected abnormal cases can be reserved as independent test cases in our proposed SCAD approach. Furthermore, we developed a cycle-consistency guided encoder to improve classification accuracy and a simultaneous optimization strategy to train the encoder and generator to reduce the inference time.

Table 1: Comparison of AUCs on test set obtained from different models

	Focal	salt	diffused	average
Anogan	0.57	0.63	0.83	0.68
Ganomaly	0.63	0.67	0.68	0.66
Ours	0.71	0.79	0.87	0.77

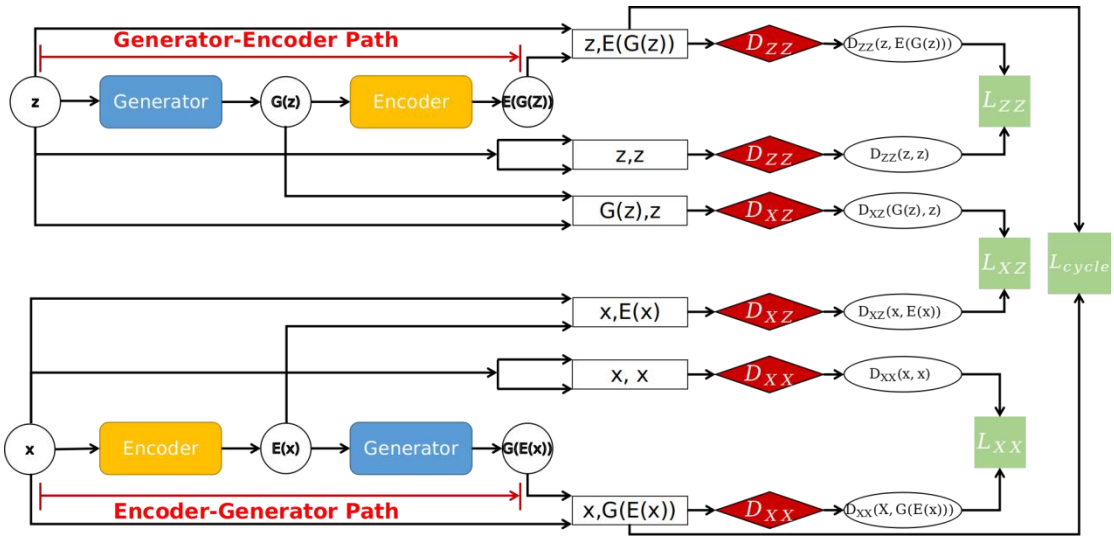

Figure 1: Training architecture of SCAD.

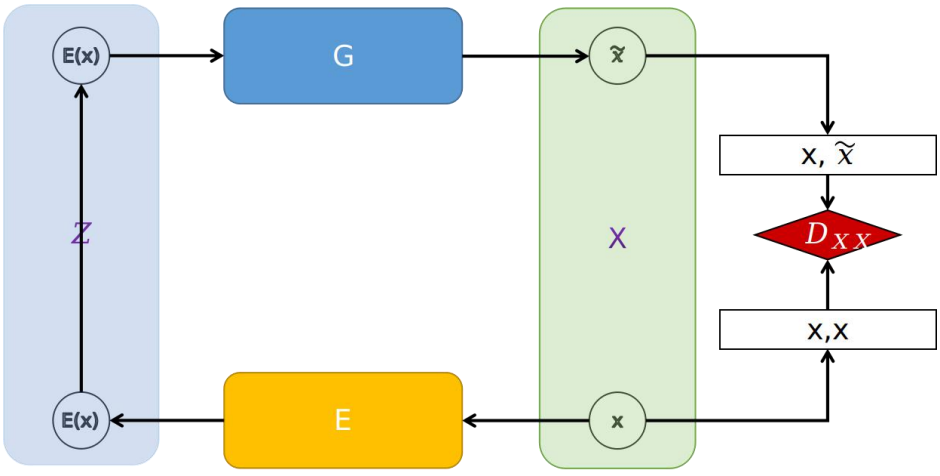

Figure2: Inference architecture of SCAD

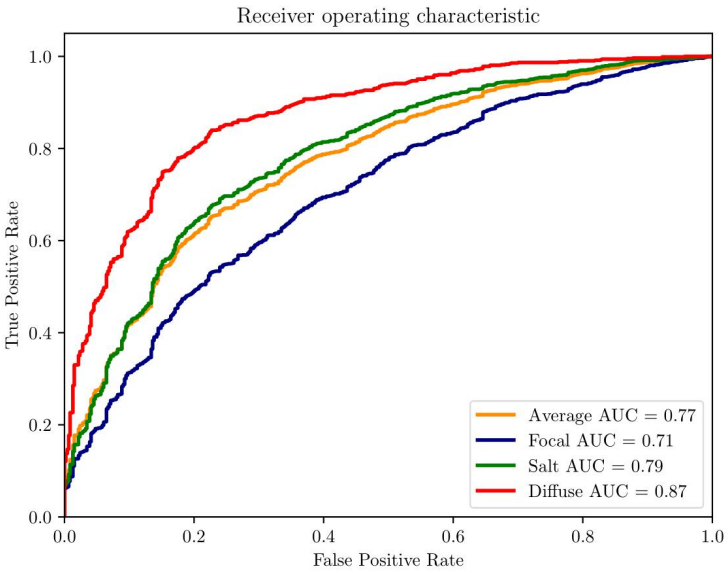

Figure 3: The ROC curves of SCAD on test set.

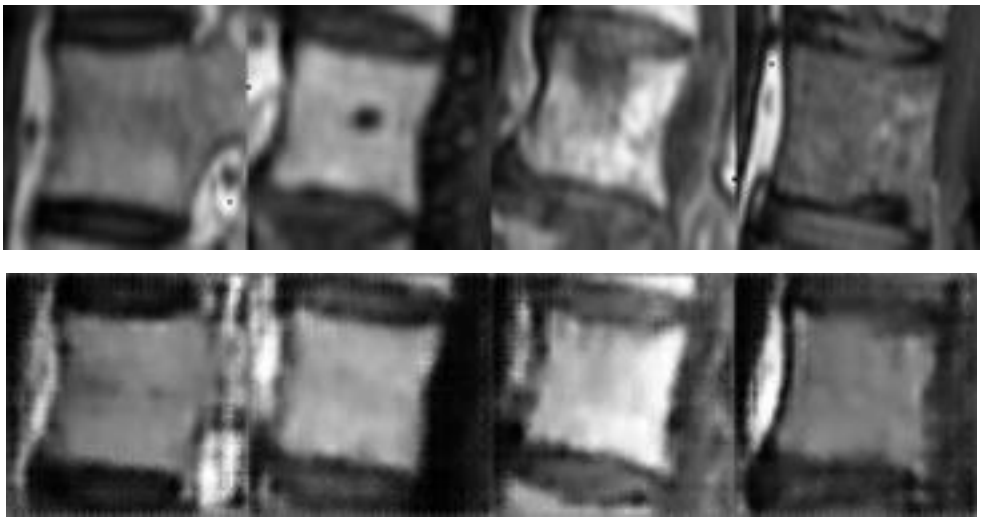

Figure 5: Examples of vertebra images generated by the proposed SCAD model . Top row: the original images. The vertebras from left to right were identified as normal, focal, variegated, and diffused patterns by radiologist. Bottom row: the reconstructed one. The SCAD was trained to reconstruct vertebras as “normal” patterns and the difference between the input and the reconstructed images as estimated by the discriminator differentiated the input from the normal pattern.